Rapidly moving sources of upper band ELF/VLF chorus near the magnetic equator.

M. Platino, U.S. Inan, T.F. Bell, J.S. Pickett, P. Canu

Rapidly moving sources of upper band ELF/VLF chorus near the magnetic equator

M. Platino,[1] U. S. Inan,[1] T. F. Bell,[1] J. S. Pickett,[2] and P. Canu[3]

Received 10 October 2005; revised 6 May 2006; accepted 2 June 2006; published 27 September 2006.

[1] Multiple simultaneous wideband (Gurnett et al., 2001) measurements on the Cluster spacecraft of upper band chorus emissions near the magnetic equator (at magnetic latitudes between $-20°$ and $10°$ and L shells ranging between L = 4 and L = 5) are used to deduce the properties of the compact source regions of ELF/VLF chorus emissions. The frequency differences exhibited by the same chorus emissions observed on different spacecraft are interpreted (Inan et al., 2004) in terms of a differential Doppler shift, using a simple model involving rapidly moving sources traveling at speeds comparable to the parallel resonant velocity of counter-streaming gyroresonant electrons. Cluster observations are used to determine the location and extent along the Earth's magnetic field lines of the source of chorus. Frequency and time differences between spacecraft are interpreted as a direct consequence of the rapid motion of highly localized source regions of chorus. In this paper, we examine the previously presented model of rapid motion of sources of chorus, extending the calculations to a three-dimensional space, using measurements of the four Cluster spacecraft. These calculations of source location and velocity as a function of frequency indicate that chorus sources move a distance of $\sim$6000 km along the field lines. The emitted chorus waves at the source are assumed to have a wide range of wave normal angles, but the rays reaching the spacecraft seem to be the ones with lower angles (with some exceptions). The ranges of velocity obtained vary with frequency around values ranging from $\sim$0.01c to $\sim$0.04c.

Citation: Platino, M., U. S. Inan, T. F. Bell, J. S. Pickett, and P. Canu (2006), Rapidly moving sources of upper band ELF/VLF chorus near the magnetic equator, *J. Geophys. Res.*, *111*, A09218, doi:10.1029/2005JA011468.

1. Introduction

[2] Chorus emissions are one of the most intense form of whistler mode plasma waves found in the Earth's near magnetosphere [*Gurnett and O'Brien*, 1964], at frequencies between a few hundreds of hertz to several kHz. They are distinguished as discrete elements, each of which lasts for a time on the order of a tenth to a few tenths of a second. In each of these elements, the frequency changes with an approximately linear rate of a few kHz/s. Chorus usually consists of rising tones, but falling tones and "hooks" are also often observed [*Burtis and Helliwell*, 1976]. These very intense natural emissions have been studied for several decades [*Helliwell*, 1965; *Dunckel and Helliwell*, 1969; *Omura et al.*, 1991; *Sazhin and Hayakawa*, 1992]. The generation mechanism of chorus waves is not yet understood, especially in terms of the underlying physical reasons for the discrete forms, frequency-time shapes, and very high growth rates. Nevertheless, it is generally believed that chorus emissions are generated via a nonlinear process [*Nunn et al.*, 1997; *Trakhtengerts*, 1999] based on the electron cyclotron resonance of whistler mode waves with energetic electrons [*Kennel and Petschek*, 1966; *Helliwell*, 1967], taking place in the vicinity of the geomagnetic equatorial plane [*Burtis and Helliwell*, 1969; *Burton and Holzer*, 1974; *LeDocq et al.*, 1998; *Lauben et al.*, 2002]. Chorus is generally observed in two frequency bands [*Burtis and Helliwell*, 1976], separated by a narrow band of decreased intensity at around one half of the local electron cyclotron frequency. Chorus waves studied in the present paper were observed at frequencies above this gap of decreased intensity, typically referred as "upper band chorus."

[3] Recent experimental work has been directed toward the localization of the source region [e.g., *LeDocq et al.*, 1998; *Parrot et al.*, 2003], propagation and time-frequency characteristics of chorus [e.g., *Nagano et al.*, 1996; *Gurnett et al.*, 2001] and determination of the properties of the chorus source [e.g., *Skoug et al.*, 1996; *Lauben et al.*, 1998]. Nevertheless, simultaneous observations of chorus emissions on multiple Cluster satellites revealed the surprising result that some individual chorus elements were observed at different frequencies on different spacecraft [*Gurnett et al.*, 2001]. This behavior was interpreted by *Inan et al.* [2004], in terms of the rapid motion of the compact source

[1]STAR Laboratory, Stanford University, Stanford, California, USA.
[2]Department of Physics and Astronomy, University of Iowa, Iowa City, Iowa, USA.
[3]Centre d'Etudes des Environnements Terrestres et Planétaires, Centre National de la Recherche Scientifique, Université Versailles Saint-Quentin-en-Yvelines, Vélizy Villacoublay, France.

0148-0227/06/2005JA011468

region(s) of chorus, leading to the observed frequency differences via Doppler shift, due to the dependence of the whistler mode refractive index on the wave normal angle ψ, the angle between the wave vector $\mathbf{k}$ and the static magnetic field $\mathbf{B}_0$. The possibility of drift motion of the chorus source region was discussed explicitly by *Helliwell* [1967] based on heuristic arguments, noting that such drifts could occur either in the direction of chorus propagation or opposite to it, and at speeds ranging from zero to the wave group velocity or parallel velocity of the resonant electrons.

[4] The generation mechanism of chorus waves in the source region, especially the highly coherent discrete forms, is not yet well understood. *Nunn* [1974] proposed a theory for the generation of chorus based on nonlinear trapping of energetic electrons, part of which has been used to explain certain features of discrete chorus waves via computer simulation [*Nunn et al.*, 1997], finding that nonlinear growth rates can be larger than linear ones by a factor of 2–5. However, it should be noted that such nonlinear theories exclusively consider an absolute instability responsible for rapid wave growth everywhere in the source region [*Nunn et al.*, 1997; *Smith and Nunn*, 1998; *Trakhtengerts*, 1999] and thus do not take into account the compact form [*Santolík et al.*, 2003, 2004; *Santolík and Gurnett*, 2003] or any motion [*Inan et al.*, 2004] of the source region. In addition, nonlinear trapping requires high wavefield amplitudes, which are eventually attained by chorus elements at the termination of their rapid growth, but the spontaneous initiation of chorus emission must necessarily occur with much smaller wavefields, basically at the levels of ambient noise.

[5] In this paper we expand on the idea presented by *Inan et al.* [2004] by analyzing the propagation of chorus for two cases during a period of moderate geomagnetic disturbance (24 July 2003). We develop a general formulation for unambiguous determination of the chorus source region and its speed of motion from measurements of the same discrete emissions on three or four spacecraft. We expand and generalize the model described previously by *Inan et al.* [2004] to three dimensions, relaxing the original assumptions and demonstrating that the location of the source can be identified by taking into account the simultaneous wideband (waveform) observations of chorus waves by four Cluster spacecraft in regions near the geomagnetic equator at a radial distance of $\sim$4.5 R_E. This analysis is mainly based on high-resolution measurements of the wideband (WBD) wave instruments [*Gurnett et al.*, 1997], and data from the Whisper sounders [*Décréau et al.*, 1997] to determine the local plasma density. In section 2, we describe the theory behind the determination of the source location, using known properties of whistler mode waves propagating in a magnetoplasma. We also briefly review previous observations of rapid motion of chorus wave sources as reported by *Inan et al.* [2004]. In section 3 we present our observations and in section 4 the results of our three-dimensional calculation of the location of the source region and the determination of its velocity.

2. Theory and Previous Work

[6] In this section we consider the Doppler shifts that would be expected to result from source region motion and illustrate how this effect would lead to the observation of individual wave packets (emanating from the same compact source region) at different frequencies on two different spacecraft. We also describe the method by which we can use the measured values of differential Doppler shift and time delay to uniquely determine the location of the chorus source region as a function of time. We include a brief summary of the first application of this method by *Inan et al.* [2004], based on two spacecraft measurements by the WBD instrument. We then describe the expansion of this method to four spacecraft measurement such as those one presented on this paper.

[7] Throughout this paper, ψ is defined as the polar angle between the wave vector $\mathbf{k}$ and the Earth's magnetic field $\mathbf{B}_0$. Since this angle is defined in a three-dimensional (3-D) space, a fixed value of ψ does not completely define the direction of $\mathbf{k}$, without the knowledge of the azimuthal direction of the vector in the plane perpendicular to $\mathbf{B}_0$. Since we deal with propagating waves, ψ can only have values $0 < \psi < \psi_{res}$, or $\pi - \psi_{res} < \psi < \pi$, where ψ_{res} is the wave normal angle at which the $\mathbf{k}$ vector approaches infinity for propagation in the whistler mode at frequencies higher than the lower hybrid resonance ($\omega > \omega_{LH}$). It should be noted that for $\psi = 0$, $\mathbf{k}$ and $\mathbf{B}_0$ are parallel and for $\psi = \pi$, $\mathbf{k}$ and $\mathbf{B}_0$ are antiparallel.

[8] *Inan et al.* [2004] interpreted the observation of frequency differences between individual discrete chorus elements observed on different Cluster spacecraft in terms of Doppler shifts resulting from source region motion. The case studied in that paper was from a time when the Cluster spacecraft passed through perigee at a radial distance of 3.85 R_E, at 0641 MLT and close to the magnetic equatorial plane, on 27 November 2000. The maximum *Kp* index was 6 in the preceding 24 hours. Figure 1a shows the basic principle of the *Inan et al.* [2004] model, where a compact source is assumed to be located along the same field line as one of two satellites (SC2), so that waves emanating at $\mathbf{k} \| \mathbf{B}_0$ (i.e., $\psi = 0$) reach SC2 propagating with a refractive index μ_0 and a group velocity v_{g0}. The second satellite (SC1) is displaced in longitude and/or latitude as well as *L* shell, so that it is accessible from the same compact source only by waves emanating at a relatively large wave normal angle ψ, corresponding to a refractive index $\mu(\psi) > \mu_0$. (Throughout this paper subscript index 0 is used for parameters corresponding to waves traveling parallel to the static magnetic field $\mathbf{B}_0$; the parameters with no subscript index correspond to waves traveling at a nonzero wave normal angle ψ.) Figure 1b shows chorus emissions observed on spacecraft SC1 and SC2, highlighting the significant frequency differences observed on the two spacecraft and the differential time delay between the two spacecraft.

[9] The source velocity v_S is then related to the measured differential Doppler shift $\Delta\omega$ as

$$v_S = \frac{\Delta\omega}{\Delta k_z(\psi)} = \frac{c\Delta\omega}{(\omega\mu\cos\psi - \omega\mu_0)}. \quad (1)$$

Using cold plasma parameters representative of the Cluster observations presented by *Inan et al.* [2004], it was shown that even for modest refractive index values (e.g., $|\mu| < 100$)

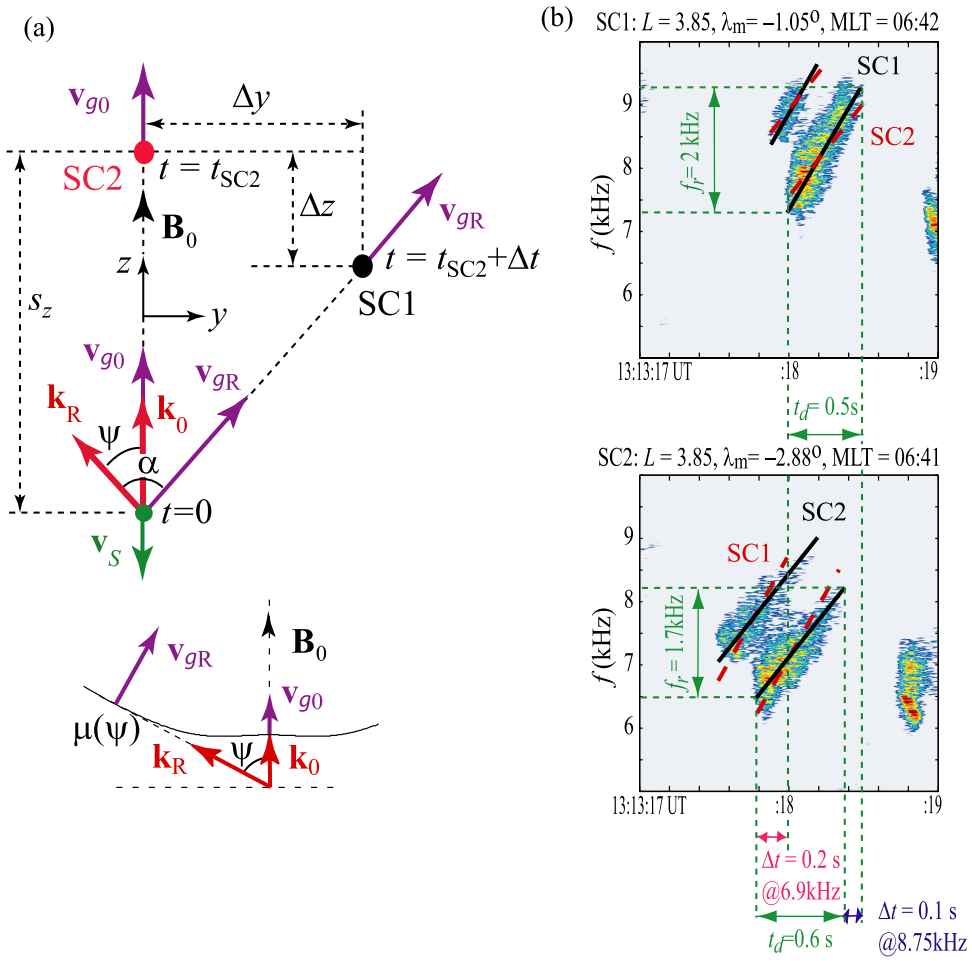

Figure 1. (a) Parameters involved in the determination of the source location with respect to the Cluster spacecraft. Highlighted are the two spacecraft SC1 and SC2, as well as the pertinent vector magnitudes of group velocity $\mathbf{v}_g$, wave vector $\mathbf{k}$, and source velocity $\mathbf{v}_S$. For the case shown, the wave arrives first at SC2 at $t = t_{SC2}$ and later at SC1 at time $t_{SC2} + \Delta t$. Included is a plot of the refractive index surface at different wave normal angle values. (b) Detailed measurement of differential Doppler frequency shift and time delay between two Cluster spacecraft for chorus elements with increasing frequency (risers) on 27 November 2000, at 1313:18 UT.

Doppler shifts observed at different wave-normal angles can differ by as much as ~1.2 kHz. Two spacecraft can thus observe individual waves originating from the same compact source at two different apparent frequencies differing from each other by the amount of the differential Doppler shift of ~1.2 kHz.

[10] According to this model, different observers would in general observe any discrete chorus wave packets emitted at the source at slightly different times, based on the dependence of the whistler mode group velocity on wave normal angle ψ. Differential Doppler shift would result in those cases when the observers are displaced (with respect to one another) either in the radial or azimuthal direction, or both. At relatively short distances from the source, when the whistler mode ray paths can be taken to be simple straight lines, the differential Doppler shift and time delay are only a function of the wave normal angle ψ.

[11] The primary conclusions and observations of *Inan et al.* [2004] were as follows:

[12] 1. The magnitude of observed differential Doppler shift and time delay are consistent with theoretical predictions for the different spacecraft separations.

[13] 2. Source velocities are comparable to either the particle parallel velocity or the wave group velocity.

[14] 3. Discrete chorus emissions appear to be produced in source regions that are compact (approximately of 1 wavelength in size or less) in the direction perpendicular to $\mathbf{B}_0$.

[15] 4. Different frequencies of individual discrete chorus elements are emitted at different points (separated by 200 to 1500 km) along the field line. Multiple, simultaneously active source(s) are likely spread out in L shell and longitude (as well as in latitude) and continually emitting waves.

[16] In the context of the *Inan et al.* [2004] model, sources of emissions are compact in the direction transverse to the field line and moving along the field line. *Santolík et al.* [2003] and *Santolík and Gurnett* [2003] examined the

18 April 2002 case also analyzed by *Inan et al.* [2004]. While the purpose of their analysis was also to determine the source region characteristics, a completely different approach was used by Santolík and coworkers. The results of *Santolík et al.* [2003] primarily concern the propagation and internal fine structure of chorus elements, while *Santolík and Gurnett* [2003] present a correlation analysis of chorus spectrograms to estimate the transverse dimensions of chorus wave packets. Differences in fine structure of the chorus elements analyzed by *Santolík et al.* [2003] can in principle be used to explain the small frequency changes observed during 18 April 2002 between chorus waves observed simultaneously in the four Cluster spacecraft. The results show fine structure inside the individual chorus elements, which is discernibly different on each spacecraft, possibly involving differences in instantaneous frequencies observed on different spacecraft. Using a parametric waveform analysis method, several examples given by *Santolík et al.* [2003] show instantaneous frequency with a resolution better than 10 Hz, so that differences of ~24 Hz as deduced by *Inan et al.* [2004] are resolvable with this method. The Doppler shift theory put forth by *Inan et al.* [2004] is not invoked by *Santolík and Gurnett* [2003] to explain the differences in frequency for this case. In this case, different magnetic field and electric field data intervals were analyzed, but no indication of a systematic Doppler shift was found.

3. Determination of Source Location and Speed From Measured Differential Doppler Shift and Time Delay

[17] In this paper, we relax the assumption of *Inan et al.* [2004] that one of the observing spacecraft is positioned along the same magnetic field line as the source region. In such a case, we know that a wave at frequency $\omega(t)$ emitted by the source, emanating from a compact source located at $z_S = s(t)$, $x_S = 0$, while moving along $\mathbf{B}_0$ at a speed $v_S = \partial s/\partial t$ in a uniform medium, can reach two different observers SC*i* and SC*j* only by propagating at two different wave normal angles ψ_i and ψ_j, and is thus observed at two different "apparent" frequencies ω_i' and ω_j', where

$$\Delta\omega_{i,j} = \omega_i' - \omega_j' = \left[k_z(\psi_i, t) - k_z\left(\psi_j, t\right)\right]\frac{\partial s(t)}{\partial t}, \qquad (2)$$

where ψ is the wave normal angle, i.e., the angle between the $\mathbf{k}$ vector and the static magnetic field $\mathbf{B}_0$. (We assign the z axis along $\mathbf{B}_0$.) In the system of coordinates used for the calculations of this paper, the origin of the x and y axis lies in the center of the Earth and the z coordinate has its origin at the magnetic equator. The positive x points toward the sun. All distances along the z axis are measured from the magnetic equator along the Earth's magnetic field lines. The location of the corresponding field line is determined by the x-y coordinates as distances to the Earth in the magnetic equator plane. Even though the lines along z in Figures 2, 4b, 5b, 7 and 8 are straight lines, they correspond to curves along the field lines of $\mathbf{B}_0$ in a regular geomagnetic system of coordinates. Distances across the field line are assumed to be perpendicular to z. Therefore the reader should see all parallel lines in the z directions as field lines located by the x-y coordinates in the magnetic equator. Distances across z, given by x and y are going to be considered perpendicular to z for locations close to the magnetic equator, i.e., for magnetic latitudes $\lambda_m \sim 0°$, considering that they are strictly perpendicular at $\lambda_m = 0°$; and locations along z are found to be in the vicinity of the equator as established for chorus waves locations in previous works (i.e., if the magnetic latitudes obtained from the calculations are within $-25° < \lambda_m < 25°$). In this sense the coordinate system can be considered as locally orthogonal in an approximate sense and distances along z are distances along field lines in close proximity to each other.

[18] We start with the assumption that the source emits waves at different values of wave normal angles with magnitudes smaller than the resonance cone angle, and that those wave packets with a specific value of ψ_i reach the corresponding SC*i* spacecraft. We then apply this assumption to all of the possible *i,j* combinations of frequency difference that can be observed with 4 spacecraft, i.e., six possible combinations, at a given frequency $\omega(t)$. The spacecraft motion can be neglected for typical spacecraft velocities (~5 km/s), since the Doppler shift due to spacecraft motion is very small for refractive indices of magnitudes smaller than 500. We assume, to a first approximation, that the wave-normal angle ψ remains constant over the assumed relatively short propagation path from the source to the observer, and we then verify this assumption using ray tracing for the given case. In case the distance from the source to the spacecraft becomes close to 1 R_E, as in our case 2 illustrated below, we correct the wave normal angle obtained using ray tracing, estimating the correct value of it for the given distance and by recalculating this distance. From equation (2) we can use the measurements of differential Doppler shift ($\Delta\omega_{i,j}$) between spacecraft SC*i* and SC*j* to estimate the value of the source velocities v_S:

$$v_S = \frac{\Delta\omega_{i,j}}{\Delta k_{z_{i,j}}} = \frac{c\Delta\omega_{i,j}}{\left(\omega\mu_i\cos\psi_i - \omega\mu_j\cos\psi_j\right)}, \qquad (3)$$

all of which must satisfy the premise of having the same frequency $\omega = 2\pi f$ at the generation region, i.e., the frequency observed at SC*i*, ω_i', must be equal to the frequency at the source plus the Doppler shift $\Delta\omega_i$. This condition can be satisfied if we add another set of equations to be satisfied for each of the four spacecraft SC*i*.

$$\omega_i' = \omega + \Delta\omega_i = \omega + \omega\mu_i\frac{v_S}{c}\cos\psi_i. \qquad (4)$$

The six equations obtained from equation (3) and the four resulting from equation (4), are part of the system of equations we use to calculate the position of the source location at a given frequency ω. Both sets are not independent, i.e., equation (3) can be derived from equation (4). Nevertheless, due to the nonlinear nature of the equations involved, the inclusion of both sets is necessary for the numerical calculation, since a solution can be found that does comply with one set but not the other one. The value of the refractive index μ_i is uniquely

given by the following relation for whistler mode waves [*Stix*, 1962, p. 38]:

$$\mu_i^2 = 1 - \frac{2(a_i - b_i + h)}{2a_i - b_i - \sqrt{b_i^2 - 4a_i h}}. \tag{5a}$$

The parameters a, b and h are obtained from

$$\begin{aligned} a_i &= s\sin^2\psi_i + p\cos^2\psi_i, \\ b_i &= rl\sin^2\psi_i + ps(1+\cos^2\psi_i), \\ h &= prl, \end{aligned} \tag{5b}$$

where r, l, p and s are obtained from the values of plasma frequency $\omega_{p\ u}$ and gyrofrequency $\omega_{c\ u}$ for each species u:

$$\begin{aligned} r &= 1 - \sum_u \left[\frac{\omega_{p_u}^2}{\omega^2}\frac{\omega}{(\omega+\omega_{cu})}\right], \\ l &= 1 - \sum_u \left[\frac{\omega_{p_u}^2}{\omega^2}\frac{\omega}{(\omega-\omega_{cu})}\right], \\ p &= 1 - \sum_u \left[\frac{\omega_{p_u}^2}{\omega^2}\right], \\ s &= \frac{r+l}{2}. \end{aligned} \tag{5c}$$

Our calculations apply to frequencies near $\omega_{ce}/2$ for which ion effects are negligible; we have therefore used $u = e$ (for "electron") and the corresponding electron plasma frequency and electron gyrofrequency. In the rest of the article we omit the u subscript and refer to these quantities simply as ω_p and ω_c.

[19] A similar construction can be carried out for the time delay ($\Delta t_{i,j}$), using the observed time difference between spacecraft SCi and SCj, leading to another group of six equations of the form

$$\Delta t_{i,j} = \frac{d_i}{v_{gi}} - \frac{d_j}{v_{gj}}, \tag{6}$$

where d_i is the distance traveled by the wave from the source to the spacecraft SCi, and the magnitude of the group velocity $v_{g\ i}$ is given by [*Helliwell*, 1965, p. 41]

$$v_{gi} \approx \frac{2c\left(\frac{\omega}{\omega_c}\right)^{\frac{1}{2}}}{\left(\frac{\omega_p}{\omega_c}\right)}\left[\frac{\tan^2\psi_i\left(\cos\psi_i - \frac{\omega}{\omega_c}\right)}{4} + \frac{\left(\cos\psi_i - \frac{\omega}{\omega_c}\right)^3}{\cos^2\psi_i}\right]^{\frac{1}{2}} \quad for\ 0 < \psi < \psi_{res} \tag{7a}$$

$$v_{gi} \approx \frac{2c\left(\frac{\omega}{\omega_c}\right)^{\frac{1}{2}}}{\left(\frac{\omega_p}{\omega_c}\right)}\left[\frac{\tan^2(\pi-\psi_i)\left(\cos(\pi-\psi_i) - \frac{\omega}{\omega_c}\right)}{4} + \frac{\left(\cos(\pi-\psi_i) - \frac{\omega}{\omega_c}\right)^3}{\cos^2(\pi-\psi_i)}\right]^{\frac{1}{2}} \quad for\ \pi - \psi_{res} < \psi < \pi. \tag{7b}$$

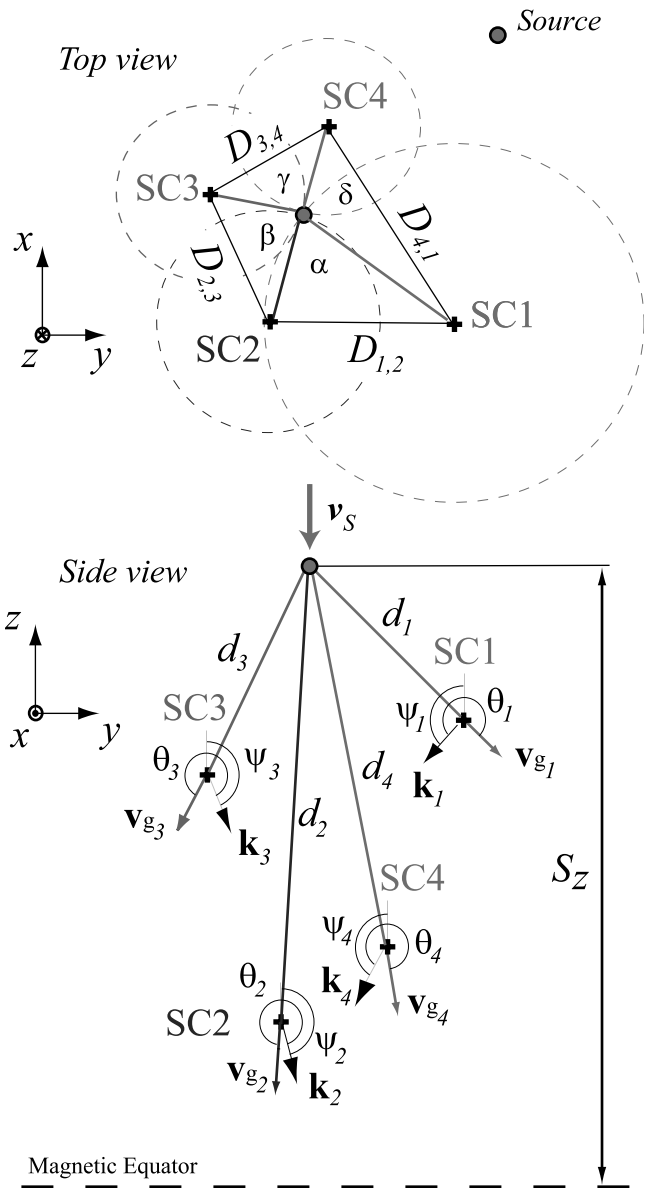

Figure 2. Schematic of the chorus emission model of a moving source, traveling along the field line. (top) Top view of the system and (bottom) side view. For i = 1...4, indicated are the wave normal angles ψ_i, distance to the source, d_i, wave vectors $\mathbf{k}_i$, source velocity $\mathbf{v}_S$, the distances perpendicular to the magnetic field lines $D_{i,j}$ between spacecraft; and source location, given by the angles α, β, γ, δ and S_Z, the component along the field line of the distance from the magnetic equator to the source. The system of coordinates in this panel is defined in section 3. The dashed circles represent all the points for each spacecraft where a source can be located at a given set of ψ_i values. The intersection of the four of them, in conjunction with S_Z, determines the unique location of the source.

Finally, to complete the set of equations, we need to take into account the geometry of the satellite locations, with respect to the source region. To illustrate this, we refer to Figure 2, showing the distance vectors d_i in different colors, from two

different points of view, and the corresponding location of the source with respect to the spacecraft. The magnitude of S_z is the projection of the distance from the magnetic equator to location of the source, along the field line.

[20] We assume that the distance from the source to the satellites is small enough to consider the propagation paths as straight lines and neglect the spacecraft motion, since it is small compared to the wave group velocity. Here we notice the distance from the source to the spacecraft d_i, and the trajectory traveled by the wave toward each spacecraft, which has an angle with respect to the static magnetic field (*z axis*) of $\theta_i - \psi_i$. The angle θ_i between the group velocity vector $\mathbf{v}_{g\ i}$ and $\mathbf{k}$ is given by [*Helliwell*, 1965, p. 41]

$$\theta_i \approx \cos^{-1}\left\{\frac{1-\frac{\omega}{\omega_c\cos\psi_i}}{\left[\frac{\tan^2\psi_i}{4}+\left(1-\frac{\omega}{\omega_c\cos\psi_i}\right)^2\right]^{\frac{1}{2}}}\right\} \quad for\ 0<\psi<\psi_{res} \tag{8a}$$

$$2\pi-\theta_i \approx \cos^{-1}\left\{\frac{1-\frac{\omega}{\omega_c\cos(\pi-\psi_i)}}{\left[\frac{\tan^2(\pi-\psi_i)}{4}+\left(1-\frac{\omega}{\omega_c\cos(\pi-\psi_i)}\right)^2\right]^{\frac{1}{2}}}\right\} \quad for\ \pi-\psi_{res}<\psi<\pi. \tag{8b}$$

The angles ψ_i are measured clockwise from the ambient static magnetic field $\mathbf{B}_0$. The angles θ_i are measured counterclockwise from $\mathbf{k}$. Equations (7a) and (8a) from *Helliwell* [1965] are defined for wave normal angles $0 < \psi < \psi_{res}$, i.e., the resonance cone angle. According to our definition of ψ these equations could not be used if $\pi - \psi_{res} < \psi < \pi$, as happens in case 2, described in the section 5. However, we know that the solution μ of equation (5a) for a given ψ is the same for $\pi - \psi$ Therefore we can use these equations redefined as equations (7b) and (8b) for $\pi - \psi_{res} < \psi < \pi$, changing the sign of the z axis.

[21] Along the z axis, parallel to $\mathbf{B}_0$, the projection of the trajectory of the waves toward each spacecraft must intersect at a single point: at the source location. This condition is fulfilled by the set of equations

$$S_z = z_{SCi} - d_i\cos(\theta_i-\psi_i) = z_{SCj} - d_j\cos\left(\theta_j-\psi_j\right) \quad i\neq j, \tag{9}$$

The value of z_{SCi} is measured as the projection of the vector location of each spacecraft in the z axis, with respect to a reference. For our calculations the origin of our coordinate system is taken to be the center of the Earth where x = 0 and y = 0 while the $z = 0$ position is located at the magnetic equator. The values of z_{SCi} are the projection in the *z axis* of the distance between each spacecraft and the magnetic equator. Equation (9) implies another set of four equations. In the *x-y* plane, at the source location S_z, the trajectories of the waves converge to one point, the field line of the source, defined by the angles α, β, γ, δ. As we see in Figure 2, the solution of this set of equations lie in the intersection of four circles, each corresponding to all of the points, which are a solution of equations (3), (4), (6), and (9) for a given set of values of d_i, ψ_i, θ_i, S_z, and which define a unique point in space in the *x-y* plane intersecting the $\mathbf{B}_0$ field line at S_z. This point is then completely specified by the angles α, β, γ, δ as follows:

$$\begin{aligned}
D_{1,2}^2 &= d_1^2\sin^2(\theta_1-\psi_1) + d_2^2\sin^2(\theta_2-\psi_2) \\
&\quad - 2|d_1\sin(\theta_1-\psi_1)d_2\sin(\theta_2-\psi_2)|\cos(\alpha), \\
D_{2,3}^2 &= d_2^2\sin^2(\theta_2-\psi_2) + d_3^2\sin^2(\theta_3-\psi_3) \\
&\quad - 2|d_2\sin(\theta_2-\psi_2)d_3\sin(\theta_3-\psi_3)|\cos(\beta), \\
D_{3,4}^2 &= d_3^2\sin^2(\theta_3-\psi_3) + d_4^2\sin^2(\theta_4-\psi_4) \\
&\quad - 2|d_3\sin(\theta_3-\psi_3)d_4\sin(\theta_4-\psi_4)|\cos(\gamma), \\
D_{4,1}^2 &= d_4^2\sin^2(\theta_4-\psi_4) + d_1^2\sin^2(\theta_1-\psi_1) \\
&\quad - 2|d_4\sin(\theta_4-\psi_4)d_1\sin(\theta_1-\psi_1)|\cos(\delta), \\
\alpha+\beta+\gamma+\delta &= 2\pi,
\end{aligned} \tag{10}$$

where $D_{i,j}$ is the distance between spacecraft SCi and SCj projected on the *x-y*, as seen in Figure 2.

[22] Now our system of equations is completely specified by the six equations from equation (3), the four equations from equation (4), the six equations from equation (6), the four equations from equation (9) and the five equations from equation (10). The unknowns for this system of 25 equations are: the frequency of the wave at the source f, the source velocity v_S, the four distances from the source to the spacecraft d_i, the four wave normal angles ψ_i, the angles α, β, γ, δ, and the source location S_z. This system of equations, even though overspecified, gives us the opportunity to take into account any errors that may exist in the measured parameters of the background plasma, such as ω_c and ω_p. We use data from the Whisper sounder instrument [*Décréau et al.*, 1997] onboard the four Cluster spacecraft to measure the plasma density, and the spacecraft magnetometer to obtain the value of $\mathbf{B}_0$, and ω_c. These values have an inherent error of approximately ± 10%, which is taken into account in the solution of our system of equations. We solve our system of equations using a minimum square error approach, with the initial values of the variables determined by trial and error, and with the constrains $|\omega_c - \omega_{c\ o}|/\omega_{c\ o} < 0.01$ and $|\omega_p - \omega_{p\ o}|/\omega_{p\ o} < 0.1$, where $\omega_{p\ o}$ and $\omega_{c\ o}$ are the observed values of the plasma and the electron gyrofrequency, respectively (The differences in the uncertainties of ω_c and ω_p are due to the difference in the methods applied to obtain them: the onboard magnetometer for ω_c and the Whisper observations for ω_p.)

4. Observations

[23] In this section we present observations of chorus on all four Cluster spacecraft on 24 July 2003, specifically from two regions before and after crossing of the magnetic equator. This particular perigee pass was selected because the spacecraft cross the equator around $L = 4$, with a spacecraft separation of no more than 580 km. The time and frequency differences between chorus elements on different spacecraft was obtained using the method of visual overlaying of 10 s long spectrograms, with a 10 Hz frequency resolution (similarly performed by *Inan et al.* [2004]). The time resolution of the WBD measurements of the electric field [*Gurnett et al.*, 1997] is ~37 μs, while the spectral overlay method yields a time and frequency resolution of ~10 ms and 10 Hz, respectively.

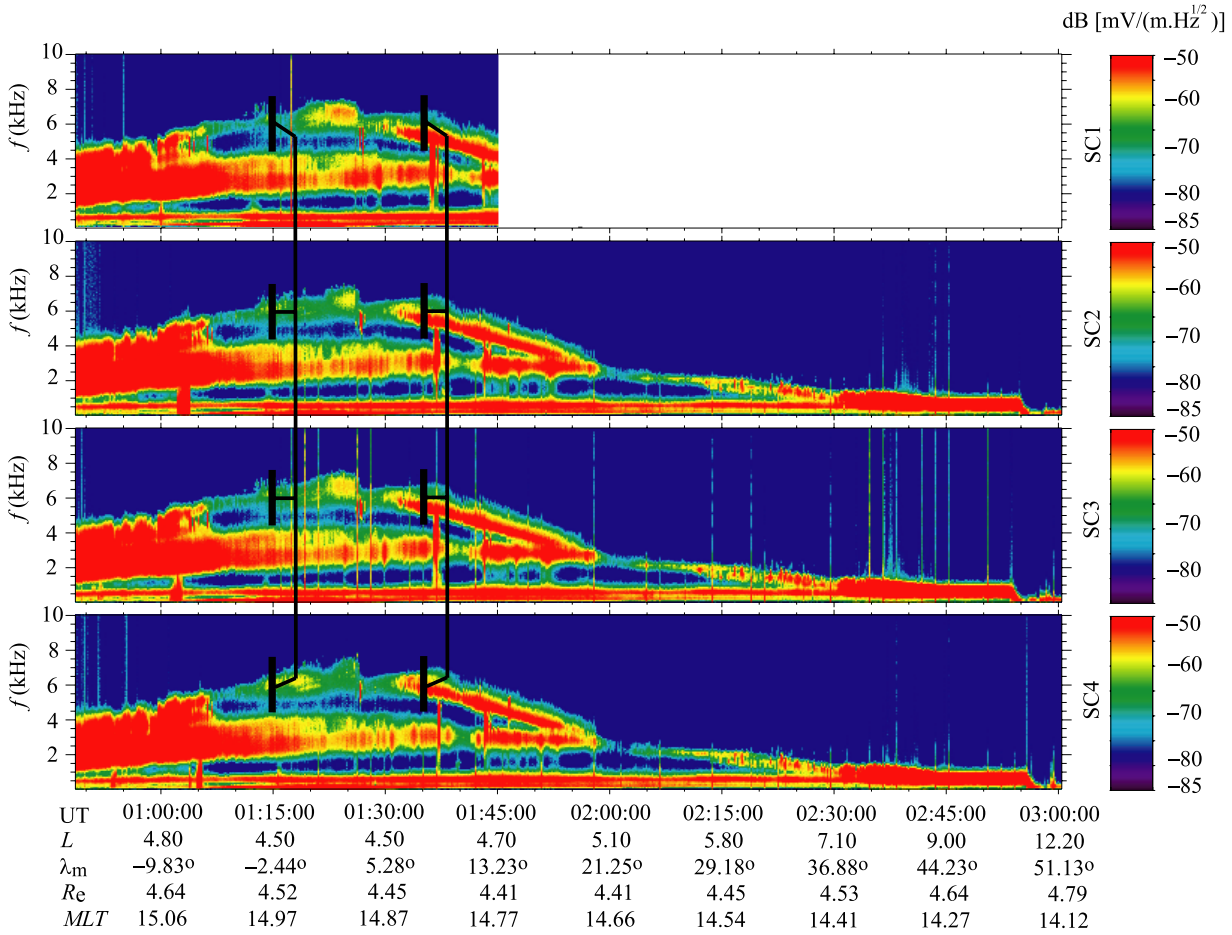

Figure 3. WBD overview spectrogram of the Cluster satellite pass during 24 July 2003, starting at 0049:00 UT. The color scale indicates the magnitude of the electric field in dB with respect to 1 mV/(m $Hz^{1/2}$). The y axis indicates frequency, and the x axis indicates universal time (UT) as well as position in formation of spacecraft SC4, in terms of the McIlwain L parameter, geomagnetic latitude λ_m, geomagnetic local time MLT, and radial distance to the center of the Earth, R_E. Highlighted are the two elements studied in cases 1 and 2, respectively.

[24] Figure 3 shows an overview of the electric field observed on the four Cluster spacecraft by the WBD instrument during 24 July 2003. Highlighted in black are the regions of the cases studied, case 1 being at 0114:38 UT and case 2 at 0135:25 UT. The four spectrograms presented in Figure 3 correspond to each of the four Cluster spacecraft, each measuring one of the components of the electric field. The *x* axis shows the universal time, as well as the geomagnetic coordinates (the McIlwain *L* parameter, the geomagnetic latitude λ as well as the radial distance R_E) of spacecraft SC4, along the path.

4.1. Case 1: 24 July 2003, 0114:38 UT

[25] Figure 4c is a 4 s long spectrogram, showing data from the region highlighted in Figure 3 for case 1, at 0114:38 UT, observed before the magnetic equator crossing during this pass. The chorus waves were observed on all four spacecraft SC1, SC2, SC3 and SC4. The frequency time spectrogram displays upper band chorus waves as observed by the four spacecraft at different times and frequencies. Displayed are the time duration and frequency span of the particular element studied in this paper. The spacecraft position with respect to one another is displayed in Figure 4b, in the system of coordinates defined in section 3. Figure 4a shows the location of the spacecraft in the frame of reference of the geomagnetic field, using the McIlwain *L* parameter and the geomagnetic latitude λ_m as a coordinate system.

[26] On the basis of the data shown in Figure 4c, we assume that individual chorus elements, i.e., chorus elements observed with distinctly similar frequency and time sequencing on different spacecraft, emanate from the same source. The difference in slope between such similar elements observed at different frequencies is also noted in Figure 4c. This difference is the result of whistler mode propagation, which introduces dispersion in frequency, as noted by *Inan et al.* [2004], and can be explained in terms of the dependence of the group velocity of whistler mode waves on the wave-normal angle ψ. The local electron gyrofrequency for cases 1 and 2 is calculated from measurements of the background magnetic field using the onboard magnetometer on each spacecraft.

[27] As discussed in section 5, the chorus source region in this case is determined to be moving toward the spacecraft.

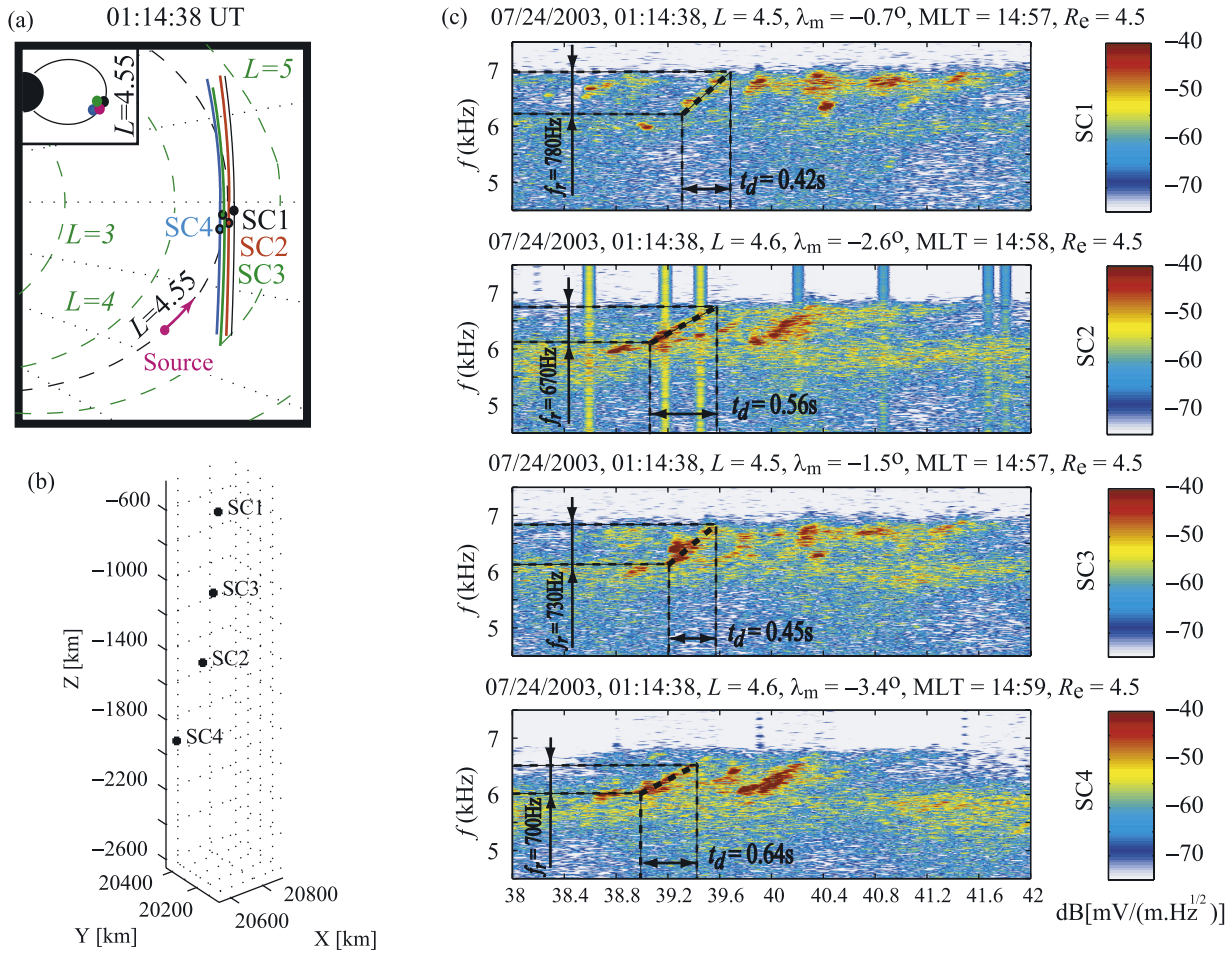

Figure 4. (a) Spacecraft location along the pass for 24 July 2003. The lines of constant L and geomagnetic latitude λ_m are indicated. Highlighted are the spacecraft located at the place in orbit when the observation was performed. (b) Relative position of the spacecraft with respect to each other in space. The system of coordinates in this panel is defined in section 3. (c) The 4 s spectrograms as observed by the four Cluster spacecraft, starting at 0114:38 UT. The color scale indicates the magnitude of the electric field in dB with respect to 1 mV/(m $Hz^{1/2}$). The *y* axis indicates frequency, and the *x* axis indicates time in UT. Highlighted is the chorus riser element studied in case 1, indicating its time (t_d) and frequency (f_r) span.

Accordingly, and for an emission in the form of a riser (rising frequency with time), the higher frequencies are emitted later in time and thus at points closer to the spacecraft. The determination of the chorus source location can now be undertaken by relaxing the assumption of having one of the spacecraft aligned with the source, as was constrained by *Inan et al.* [2004], since our system of equations is complete, allowing us to determine the source location uniquely using measurements from the four spacecraft. The direction of the source movement is also uniquely determined from the calculations described in section 5.

4.2. Case 2: 24 July 2003, 0135:25 UT

[28] Figure 5c is a 4 s long spectrogram, as highlighted in Figure 3 for case 2, at 0135:25 UT, showing data from observed after the magnetic equator crossing during the pass, illustrating the rising emissions. The chorus waves were observed on all four spacecraft SC1, SC2, SC3 and SC4. The frequency time spectrogram displays upper band chorus waves as observed by the four spacecraft at different times and frequencies. Displayed are the time duration and frequency span of the particular discrete chorus element studied in this paper. The spacecraft position with respect to each other is shown in Figure 5b, where the coordinates *x*, *y* and *z* are geomagnetic, i.e., the magnetic equatorial plane corresponds to $z = 0$ and the center of the Earth is $x = 0$ and $y = 0$. Note that the *z* axis is not exactly vertical, but that it represents the distance in km along the field line which crosses the magnetic equator at the geomagnetic coordinates given by *x* and *y*. Figure 5a shows the location of the spacecraft in the frame of reference of the geomagnetic field, using the McIlwain *L* parameter and the geomagnetic latitude λ_m as a coordinate system.

[29] As in case 1, we assume that individual distinct chorus elements, i.e., those with similar frequency and time sequencing on different spacecraft, emanate from the same source. The difference in slope between similar elements observed in different frequencies is also noted in Figure 5c, as the result of whistler mode propagation in the magnetosphere, which introduces dispersion in frequency, originat-

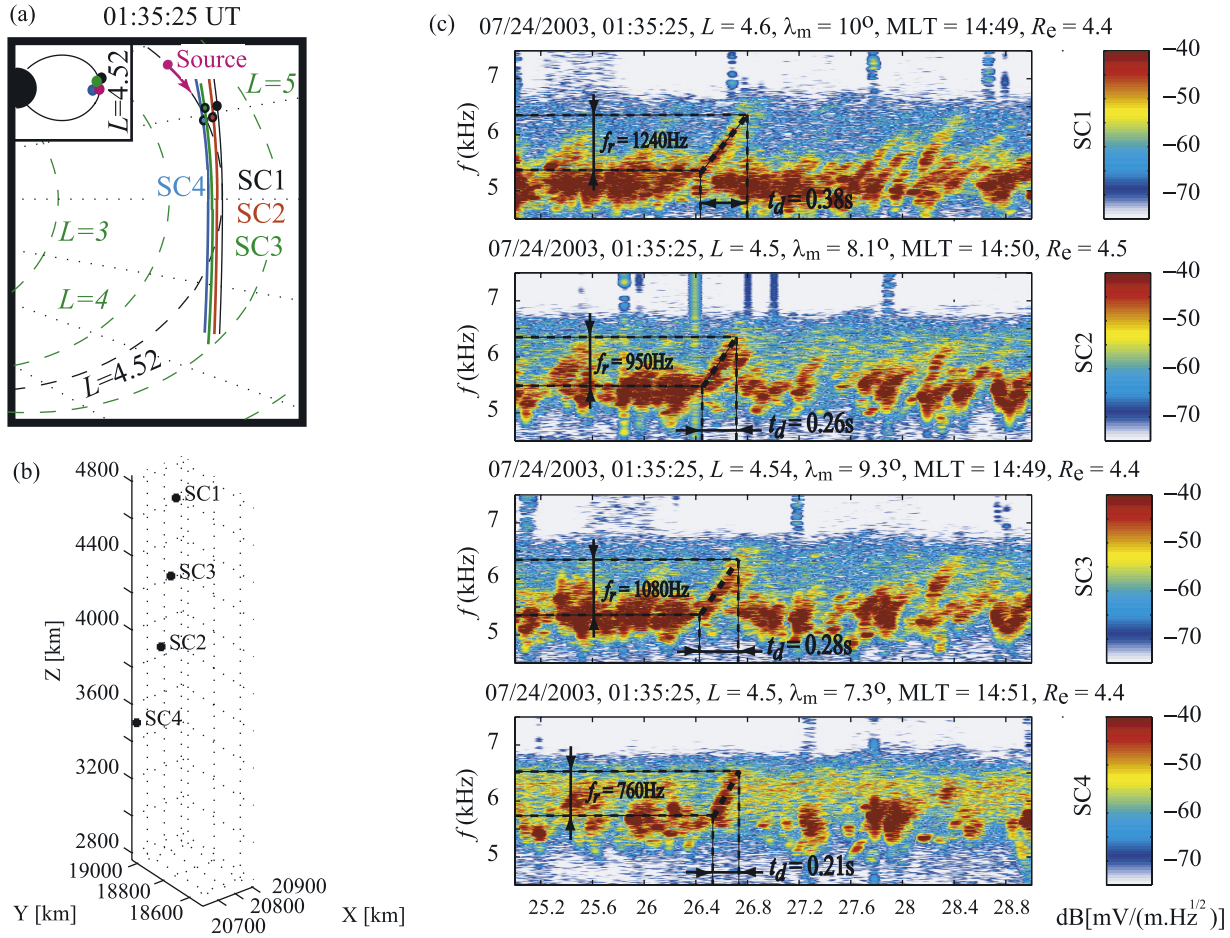

Figure 5. (a) Spacecraft location along the pass for 24 July 2003. The lines of constant L and geomagnetic latitude λ_m are indicated. Highlighted are the spacecraft located at the place in orbit when the observation was performed. (b) Relative position of the spacecraft with respect to each other in space. The system of coordinates is defined in section 3. (c) The 4 s spectrograms as observed by the four Cluster spacecraft, starting at 0135:25 UT. The color scale indicates the magnitude of the electric field in dB with respect to 1 mV/(m $Hz^{1/2}$). The *y* axis indicates frequency, and the *x* axis indicates time in UT. Highlighted is the chorus riser element studied in case 2, indicating its time (t_d) and frequency (f_r) span.

ing from the dependence of group velocity for whistler mode propagation, with frequency and the wave-normal angle ψ. The general appearance of the spectra for this case consists of a multiplicity of chorus emissions generally observed only on one of the four spacecraft, mixed in with some elements observed on some of the spacecraft but not on all of them. Figure 5 shows one particular element that was recognized to be common on all four spacecraft. Note that the fact that many elements are only observed on one spacecraft, and some on more than one and even fewer on all four is consistent with the general picture of distributed multiple active chorus sources, emitting waves in a range of directions, as described in Figure 7 of *Inan et al.* [2004].

[30] In this case, as in case 1, detailed calculations presented in section 5 indicate that the chorus sources are moving toward the spacecraft. In other words, risers are observed during this pass both before and after the equator, so that as the frequency increases with time, the higher frequencies are emitted at points later in time and thus closer to the observers. As pointed out in the previous paragraph, the important feature to note is the fact that some of the elements are observed in some of the spacecraft but not in others. In some cases we can see that part of the chorus element is observed on one of the spacecraft while the entire element is observed in another. This type of distribution of chorus elements appears to be a common feature of multi-point observations of chorus and suggests the presence of multiple, simultaneously active compact sources distributed in space as mentioned by *Inan et al.* [2004]. Chorus waves emanating from different sources sometimes reach different spacecraft, and sometimes reach all four of them. Under this situation, it can be more difficult to identify similar elements observed on different spacecraft. Nevertheless simple visual inspection indicates that chorus emissions often have a very unique frequency-time structure, and that this structure, even when shifted in frequency and dispersed (e.g., slight changes in slope), still maintains its distinct frequency-time shapes from one spacecraft to another. Visual inspection of

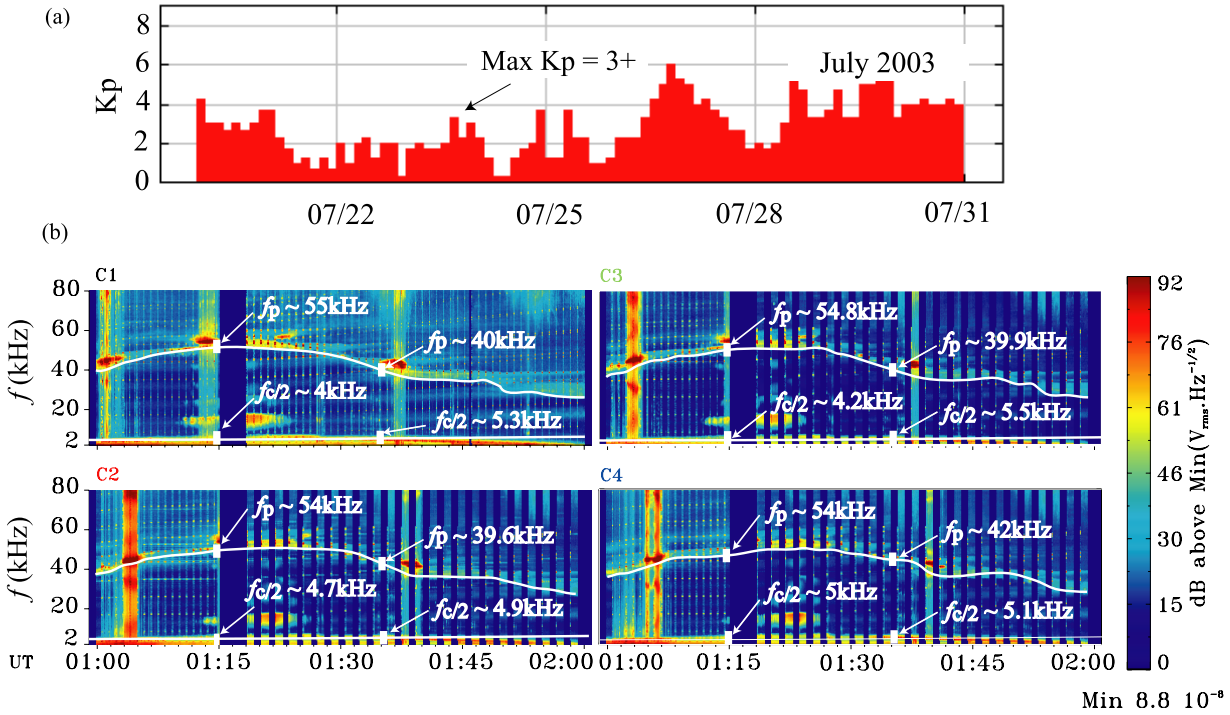

Figure 6. (a) Geomagnetic activity index (*Kp*) plot, for the last week of July 2003. Highlighted is the local maximum in the *Kp* index value, as observed in the previous 24 hours to the observations in Figure 3. (b) Whisper overview spectrogram of the Cluster satellite pass during 24 July 2003, starting at 0100:00 UT. The color scale is related to the magnitude of the electric field in dB, measured with respect to 0.088 μV/(m $Hz^{1/2}$). The *y* axis indicates frequency, and the *x* axis indicates universal time (UT). Highlighted in white are the plasma frequency f_p and $^1/_2$ electron gyrofrequency $f_c/2$ observed in each spacecraft, and the corresponding values used for the calculations in cases 1 and 2, respectively.

4 s long sections like the ones shown in Figures 4 and 5 are used to measure the frequency-time characteristic of the single elements highlighted in Figure 3, which are later used in equations (4) and (6) to estimate the variation of differential Doppler shift and time delay, respectively, as a function of time during the pass.

4.3. Geomagnetic Conditions on 24 July 2003

[31] The maximum *Kp* index observed in the 24 hours prior to the events studied here was about 3+ (The notation of a + sign after the number means that the actual value is more than 3, but less than 3.5. This notation is used in *Kp* displays since the actual value does not have more than 1 significant digit.) The variation of the geomagnetic activity, is presented in Figure 6a, showing the variation of the *Kp* index during the day before and up to two days after the observed events shown in this paper.

[32] To derive values of local plasma density, we used data from the Whisper resonance sounder [*Décréau et al.*, 1997]. Frequency-time spectrograms generated from measured electric field observations using the Whisper instrument in the passive mode [*Décréau et al.*, 1997] are shown in Figure 6b. The four panels show spectrograms of one of the components of the electric field on spacecraft SC1, SC2, SC3 and SC4, for the pass on 24 July 2003. The Whisper sounder on the Cluster spacecraft can provide an absolute measurement of the total plasma density within the range 0.2–80/cm^3, which are typical values of electron plasma density observed in the outer magnetosphere at $L \sim 4$. The data from this instrument allows the identification of the electron plasma frequency by analyzing the time-frequency patterns of resonances triggered in the medium by a pulse transmitter. The sounding technique used for this purpose was already developed and proved successful in these regions of the magnetosphere by *Etcheto et al.* [1983] and *Trotignon et al.* [1986]. In the basic nominal operational mode, as is the case presented in this paper, the density is measured every 52 s on SC1. In SC2, SC3 and SC4 it is measured in the same manner during the first 15 min and every 104 s during the rest of the event, the frequency and time resolution for the wave measurements being of about 300 Hz and 2.2 s. In the passive mode, natural wave bands between two successive harmonics of the electron gyrofrequency can be observed (see Figure 6b). We used these active and passive measurements to obtain the electron density through the method specified by *Canu et al.* [2001] and *Trotignon et al.* [2001, 2003].

5. Source Location and Velocity Results

[33] The determination of the source location and the direction of its motion, results directly from the calculation described in section 3, by solving the system of equations described by (3), (4), (6), (9), and (10) using the measured

Table 1. Guess Values $\mathbf{x}_g$ Used to Solve the System of Equations Described by (3), (4), (6), (9), and (10) for Cases 1 and 2

	$\mathbf{x}_{1g}$	$\mathbf{x}_{2g}$	$\mathbf{x}_{3g}$	$\mathbf{x}_{4g}$
		Case 1		
f, Hz	5500	5600	5700	5800
v_s, c	0.001	0.001	0.001	0.001
d_1, km	4600	3800	3500	2500
d_2, km	3600	2900	2200	1500
d_3, km	4100	3500	2800	2000
d_4, km	2900	2300	1700	1000
ψ_1, deg	4.2	5	6	15
ψ_2, deg	10	10	12	15
ψ_3, deg	6.4	7.1	8	17
ψ_4, deg	0	0	0	0
α, deg	90	90	90	90
β, deg	90	90	90	90
γ, deg	90	90	90	90
δ, deg	90	90	90	90
S_z, km	−4700	−4000	−3500	−2500
		Case 2		
f, Hz	4300	4600	5000	5200
v_s, c	−0.02	−0.033	−0.02	−0.02
d_1, km	6800	6300	5400	5200
d_2, km	7800	7200	6400	6100
d_3, km	7200	6700	5900	5600
d_4, km	8200	7700	7000	6500
ψ_1, deg	135	138	138	135
ψ_2, deg	169	160	152	146
ψ_3, deg	139	140	139	140
ψ_4, deg	180	180	180	180
α, deg	90	90	90	90
β, deg	90	90	90	90
γ, deg	90	90	90	90
δ, deg	90	90	90	90
S_z, km	11000	10500	9500	8000

values of the differential time delays and Doppler shifts (over a range of frequencies) as inputs. This solution is dominated by the time sequence of arrival of the chorus wave packet to the different spacecraft and the geometry of the problem, being the configuration in space of the four Cluster spacecraft approximately along a line in the z direction (see Figures 4b and 5b). This set of equations is highly non linear in terms of the wave normal angle ψ, and is over determined, and therefore lead to different solutions depending on the initial values used. The method used to solve this block of equation is the minimization method [*Marquardt*, 1963], which consists on defining a square error function $g(\mathbf{x})$ as

$$g(\mathbf{x}) = \sum_{n=1}^{25} \beta_n [q_n(\mathbf{x}) - r_n(\mathbf{x})]^2, \tag{11}$$

where the 25 r_n, q_n $\Re^{15} \rightarrow \Re$ are defined as each side of the equality of equations (3), (4), (6), (9), and (10) and the vectors $\mathbf{x} \in \Re^{15}$ represent the set of 15 unknowns specified in section 3, $\mathbf{x}_g$ being their respective estimated values. As an example we use equation (3) with spacecraft SC1 and SC4, therefore we will have for this case:

$$q_n(\mathbf{x}) = v_S \quad r_n(\mathbf{x}) = \frac{c\Delta\omega_{1,4}}{(\omega\mu_1(\mathbf{x})\cos\psi_1 - \omega\mu_4(\mathbf{x})\cos\psi_4)}, \tag{12}$$

where $\mu_1(\mathbf{x})$ and $\mu_4(\mathbf{x})$ must be replaced by expression (5a), with $i = 1$ and 4, respectively. For this approach to work well, we must weigh each term of the sum in equation (11) with a factor β_n, in order not to render any variable more significant than any other in the solution. The β_n values are chosen by trial and error based on the behavior of equations q_n and r_n. The values of β_n are obtained in an iterative fashion. They are chosen as the inverse of the estimated values of r_n for each guess value of the unknown vector (which we will call $\mathbf{x}_g$) raised to square power, that is $\beta_n = r_n(\mathbf{x}_g)^{-2}$. The trial and error nature of this method comes from the proper election of the $\mathbf{x}_g$, the most complicated task in the calculation, and one that can only be done by common sense and good knowledge of the physics involved in the problem. A proper selection of $\mathbf{x}_g$ will lead to convergence, a wrong set of values for $\mathbf{x}_g$ can lead to a set of solutions that leads to a minimum in the solution space, but that will not satisfy the system of equations within the limits of the tolerance on the measurables, therefore not constituting a real solution. The values of $\mathbf{x}_g$ used for cases 1 and 2 are shown in Table 1, corresponding to each of the unknowns.

[34] The system of equations can then be solved using different algorithms, the ones used for this case being the quasi-Newton [*Acton*, 1990, chapter 14; *Moré and Cosnard*, 1979] and the Levenberg-Marquardt [*Levenberg*, 1944; *Marquardt*, 1963] methods, the latter being the more efficient for the case in hand.

[35] Our method of solution relies on the measurement of the frequency and time difference as well as the frequency-time slope of the individual chorus elements observed on the four spacecraft. The manner in which this measurement is used in our determination of the source properties is illustrated in Figures 4c and 5c. The chorus emission is assumed to be generated with a linearly increasing frequency with time at the source region, which subsequently moves toward or away from the spacecraft (depending on the sign of the Doppler frequency shift) resulting in the frequency-time slopes that are observed on SC1 to SC4. The solution of the system of equations includes the original frequency range and frequency-time shape of the emission at the source, uniquely determined by the unknowns f (or ω) and the propagation times d_i/v_{gi}, with $i = 1...4$. This process also has the desired outcome of the specific location at which each frequency is emitted and the direction and the magnitude of the velocity of the source.

[36] For case 1, displayed in Figure 4, the results are shown in Figure 7. The four panels presented herein correspond to four different values of frequency f, calculated from the system of equations presented in section 2. These four points in frequency correspond to four different parts of the chorus element highlighted in Figure 4. The reason for using four frequency-time points in the chorus element is justified by noting that it is the minimum number of points by which we can take into account changes in the frequency-time slope of the element, if there should be any. For the three cases studied here we have linear slopes, therefore two points should be enough. Nevertheless we use four for completeness. The election of the points is done by picking uniformly distributed frequency-time pairs, and the impact on the error bars will depend on the spread in frequency of the element. The four measurements of this element, as observed by spacecraft SC1 to SC4, were divided in equal parts, in time and frequency, each part having a corresponding value of time and frequency. All of the six

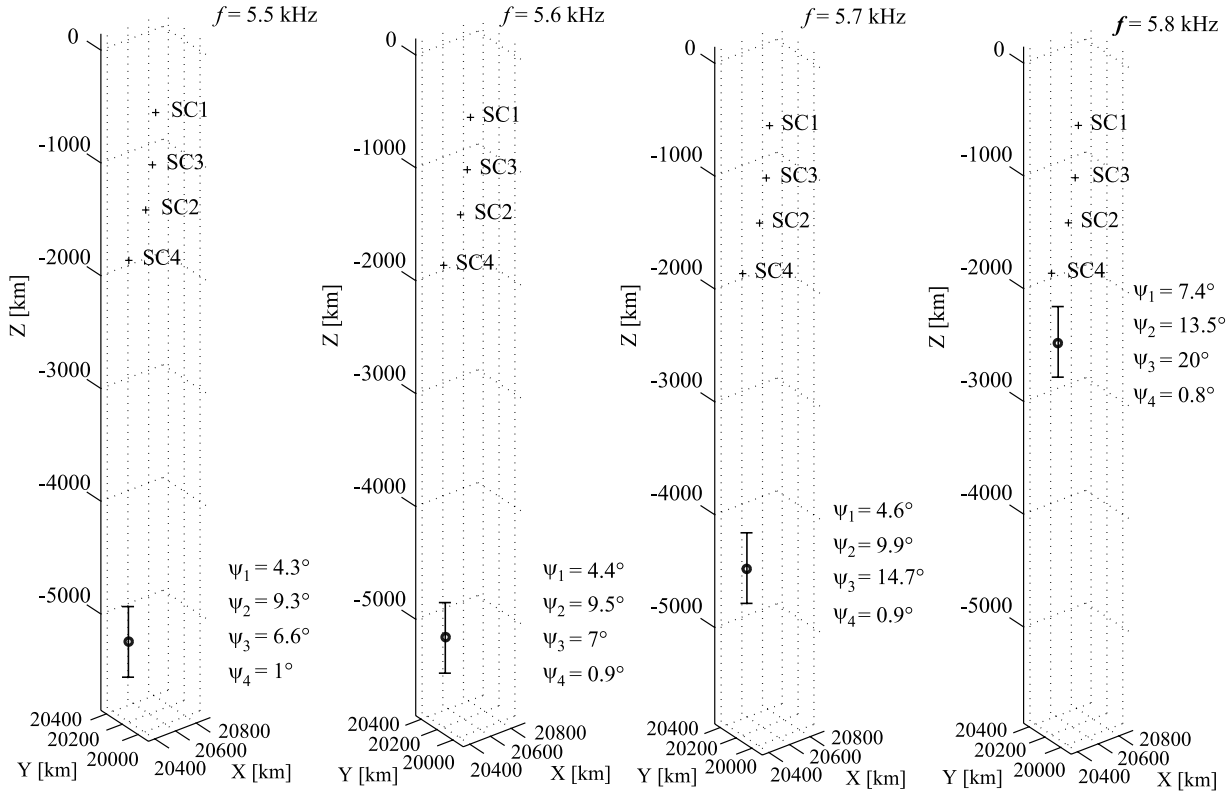

Figure 7. Source location results on 24 July 2003, 0114:38 UT, for four different calculated frequencies, each one corresponding to each of the four panels. Indicated is the position of the spacecraft as well as the source. The system of coordinates in this panel is defined in section 3. For each result in source location is specified the corresponding values of wave normal angle (ψ_i, for i = 1. . .4).

combinations of pairs from these four values of f_i and t_i, for each spacecraft SC*i*, are fed into equations (4) and (6) to calculate the values of $\Delta\omega_{i,j} = \omega_i - \omega_j$ and $\Delta t_{i,j} = t_i - t_j$, the index *i* and *j* representing the corresponding number of spacecraft SC*i* and SC*j*. As explained at the end of section 2, the values of the plasma frequency ω_p and the electron gyrofrequency ω_c, are also considered as unknowns and restricted to a range of $|\omega_c - \omega_{co}|/\omega_{co} < 0.01$ and $|\omega_p - \omega_{po}|/\omega_{po} < 0.1$, where $\omega_{po} = 54.5$ kHz and $\omega_{co} = 8$ kHz for case 1, as highlighted in Figure 6. $\Delta\omega_{i,j}$ and $\Delta t_{i,j}$ also have their respective uncertainties and should also be considered as unknowns with the restrictions $|\Delta t_{i,j} - \Delta t_{i,jo}| < 0.01$ s and $|\Delta\omega_{i,j} - \Delta\omega_{i,jo}|/2\pi < 10$ Hz (the subindex *o* refers to the observed values of ω_c, ω_p, $\Delta t_{i,j}$ or $\Delta\omega_{i,j}$). We use these tolerance values for the four measurables, ω_c, ω_p, $\Delta\omega_{i,j}$ and $\Delta t_{i,j}$ in the two cases studied in this paper. The results in Figure 7 show the values of the location of the source as given uniquely in the 3-D space by S_z, d_1 to d_4, and the set of angles α, β, γ, δ (see Figure 2). The error bars in the *z* direction are obtained from equation (9), representing the range of values acquired by S_z for different values in the solution space, within the restrictions mentioned earlier. The system of equations is expected to have several solutions, and we find that such is indeed the case, but the solutions found must also have physical significance and within those ones that are found, the one with a minimum value of $g(\mathbf{x})$ is the one that is adopted to be the solution.

[37] The concept of a moving source is linked to the result of having different values of source location for different values of frequency. Also we must note that the source seems to be moving toward the observing spacecraft, traveling a distance between the locations at which the lowest and the highest frequencies are generated, of ~2500 km. Previous chorus observations, such as those documented by *Lauben et al.* [2002], suggest that the location of the source of chorus waves lies in the vicinity of the magnetic equator, while *Inan et al.* [2004] deduced a moving source located within ~5000 km of the equatorial plane. *Lauben et al.* [2002] found that the generation of chorus waves occurs at wave normal angles for which the wave group velocity vector is parallel to the magnetic field lines. This may occur at values of $\psi = 0°$, or $\psi = \psi_G$, being ψ_G the so-called Gendrin angle [*Gendrin*, 1974]. Such wave normal angles lead to ray paths (i.e., direction of wave group velocity) that tend to stay parallel to the magnetic field lines, for latitudes near the magnetic equator. For the cases studied there, the sources were found to be located in the vicinity of the magnetic equator, where the static magnetic field exhibits a minimum inhomogeneity. This result agrees with previous estimations of source location [*Burtis and Helliwell*, 1969, 1976; *LeDocq et al.*, 1998; *Santolík et al.*, 2003; *Parrot et al.*, 2003] where source locations of dayside chorus in geomagnetic latitudes, was found to be located within −25° and 25° of the magnetic equator. *Lauben et al.* [2002] concluded that sources located at large distances from the spacecraft must emit chorus waves at these wave normal angles, otherwise they tend to diverge away from the field lines, while waves emitted at

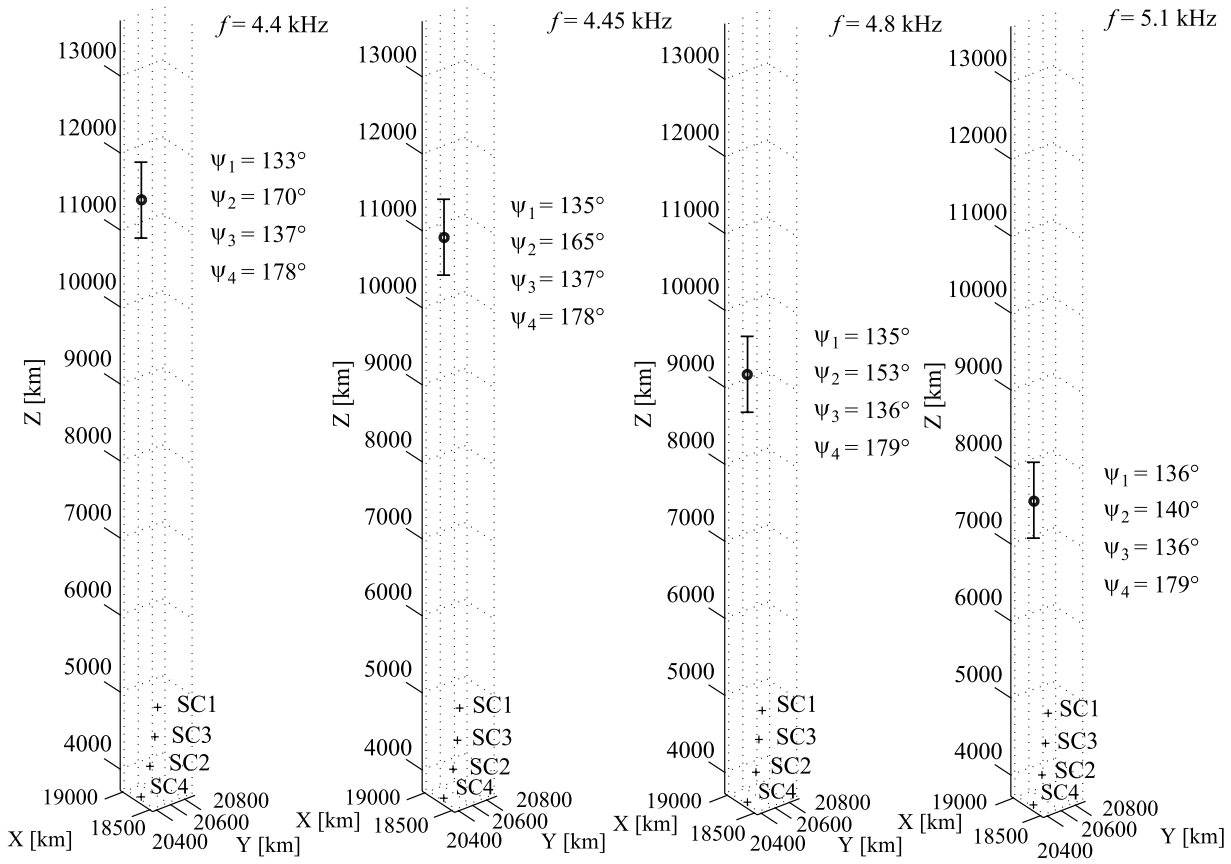

Figure 8. Source location results on 24 July 2003, 0135:25 UT, for four different calculated frequencies, each one corresponding to each of the four panels. Indicated is the position of the spacecraft as well as the source with their corresponding error bars along the z axis. The system of coordinates in this panel is defined in section 3. For each result in source location is specified the corresponding values of wave normal angle (ψ_i, for i = 1. . .4).

the Gendrin wave normal angle tend to remain more tightly focused and provide a coherent illumination over large distances than do waves at other angles, in the absence of field aligned plasma irregularities. Furthermore, the fact that the wave energy stays along the field line to which the resonant electrons are also confined to, may be important in the generation mechanism of these emissions.

[38] The chorus element studied in case 2, displayed in Figure 5, is found to have a source region as shown in Figure 8. As in case 1, the four panels correspond to four different values of frequency f, which were calculated from the system of equations presented in section 3. This result also suggests a field aligned moving source, emitting coherent wave packets at different frequencies at different locations along the field line. These four values of f, were calculated using the same method of dividing the chorus element into four f-t pairs, as explained before. The results on Figure 8 display the values of the location of the source as given uniquely in the 3-D space by S_z, d_1 to d_4, and the set of angles α, β, γ, δ (see Figure 2). As in case 1, the error bars in the z direction are obtained from equation (9), being the deviation on S_z for different values in the solution space, within the restrictions mentioned earlier. In this case, the system of equations is also expected to have several solutions as before. The solutions found must have physical significance and within the ones that do, the one with a minimum value of $g(\mathbf{x})$ is adopted. Results shown in Figure 8 suggest that the risers observed in Figure 5 are generated away from the equator, while the sources of the emissions move rapidly toward it. The extent of the source along the field line is larger for case 2, being ~3700 km, while the frequency range spanned by the risers in Figure 5 is more than that for the risers in Figure 4. The source region in this case is also moving toward the spacecraft, i.e., in the direction of propagation of the chorus wave packets.

[39] Results shown in Figures 7 and 8 have been obtained using the formulation and the method of calculation presented in section 2. These calculations are performed based in the fact that rays propagate roughly along the field line, and that the wave normal angles do not change much along their trajectory. Nevertheless the source-to-spacecraft distances obtained are found to be large enough to raise questions about the validity of this assumption. To assess the possible effects of wave normal angle variation (along the path) on our results, the calculation is repeated using ray tracing in an inhomogeneous magnetospheric model to estimate the values of the wave normal angles and to correct the values of the source location accordingly. The ray-tracing method used is described by *Platino et al.* [2005] and consists of the use of the plasma density profile

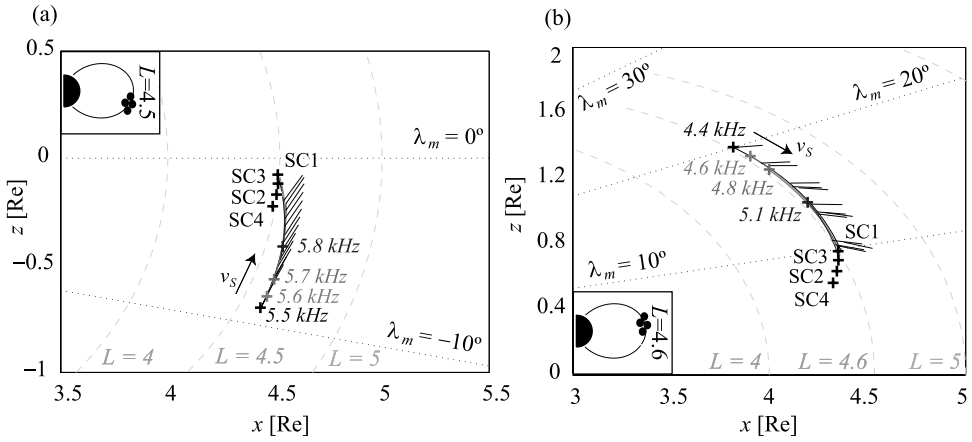

Figure 9. Ray-tracing results for 23 July 2003, when rays are launched from the source locations calculated for each of the four frequencies obtained in this case. The solid lines correspond to each frequency ray path, while the small black segments placed periodically along the ray path represent the direction of the wave vector, **k**. Displayed are the lines of constant L and geomagnetic latitude λ_m.

obtained from the Whisper instrument, as an input to the Stanford ray-tracing program described by *Inan and Bell* [1977]. The waves are launched from the positions calculated using the model developed in this article, with the values of frequency and wave normal angle obtained by the system of equations in section 2. The resultant propagation times from the source to the spacecraft are compared to the measured values and an adjustment in the values of ψ_i for each spacecraft SC*i* is performed in order to fit the measured delays. Even though this process may result in slightly different values of f, ψ_i, d_i, S_Z and α, β, γ, δ, than the ones calculated originally, the changes are not significantly high, as can be seen from Figure 9. Here we see the evolution of ψ_i for chorus rays launched from the estimated source toward the spacecraft SC*i*, in both cases, 1 and 2 (The distances between spacecraft are exaggerated for clarity). The continuous lines indicate the ray trajectories for different frequencies while the small black segments show the direction of the wave **k** vector. Indicated in Figure 9 are the values of the wave normal angles at the source and at the spacecraft. The correct values of the source location and velocity, displayed in Figures 7, 8, and 10 are calculated taking into account the effect of ray propagation as described in this paragraph and shown in Figure 9.

[40] The results of calculated source velocities are shown in Figures 10a and 10b, which show the source velocity for the values of frequency obtained from the calculations described on Figures 7 and 8. The error bars on Figure 10 are calculated considering the sensitivity of the solution on changes on the values of the input parameters of ω_p and ω_c. Superimposed on the source velocity plot are the corresponding values of the parallel velocity of resonant energetic electrons for $\psi \approx 0$, as calculated from [*Helliwell*, 1967]

$$v_S = -v_{\parallel} = \frac{\omega_c - \omega}{k} \cong \frac{(\omega_c - \omega)^{3/2}}{\omega_p\ \omega^{1/2}}. \qquad (13)$$

The source velocities calculated for both cases differ within a factor of ~3, being higher for the risers observed after the equatorial crossing. In case 1 the source velocity increases with frequency, while in the second case it decreases.

6. Summary

[41] This study of chorus emissions and their source regions was motivated initially based on the interesting characteristics reported by *Gurnett et al.* [2001], where chorus waves were observed in two different spacecraft at different frequencies. This effect was initially interpreted [*Inan et al.*, 2004] to be the cause of the Doppler frequency shift, of the signal propagating form the source toward the spacecraft. In that article, the authors were able to estimate a source size and an approximate location with respect to the spacecraft. In the present work, we expand this study, using measurements from the 4 spacecraft provided by the WBD instrument, to uniquely locate the chorus source in space, calculating wave group velocity and source velocity form differential Doppler frequency shifts and time delays observed on board the spacecraft. To that extent, we present two cases observed during 24 July 2003, where the upper chorus band can be observed showing an increase of intensity and dropping suddenly around the geomagnetic equator (Figure 3). This high variability is seen almost on every perigee pass of Cluster in the WBD instrument. It is also noted in the more detailed Figures 4 and 5 the frequency characteristic of upper band chorus, in this case as risers that last for about 0.4 s, but the same element is seen with different frequency time characteristic on different spacecraft. A detailed method for estimating the source location and motion in space based on Doppler shift analysis is presented.

[42] The results of our source location calculations are consistent with compact transverse size of the source, while the emission of different frequencies of the same element occurs over an extended region along the field line. This idea reinforces the interpretation of source region motion given by *Inan et al.* [2004], where discrete chorus emissions are produced in source regions which are highly compact (of the order of one wavelength, or tens of kilometers) in the

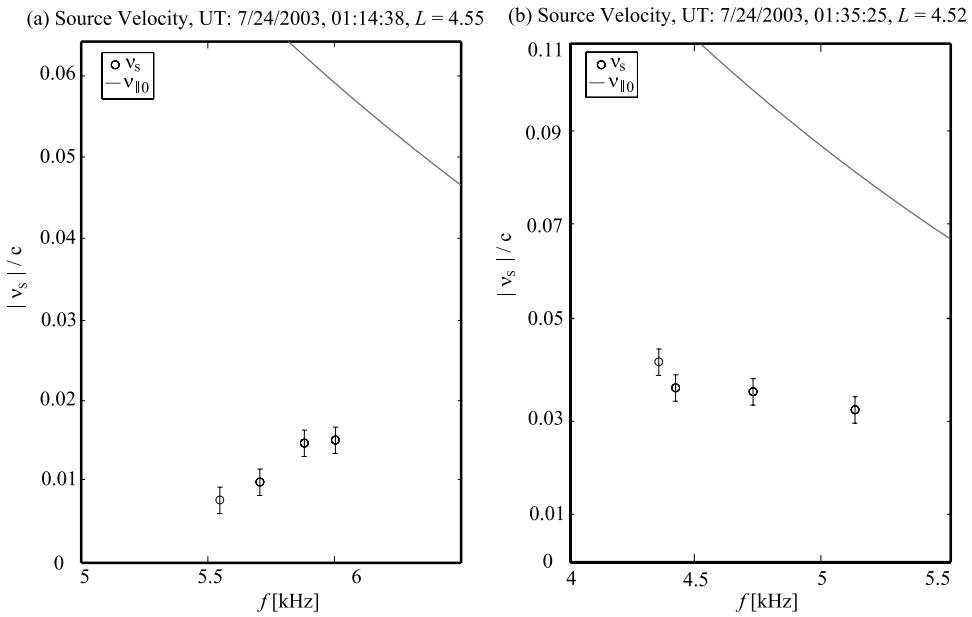

Figure 10. Results of the calculations of source velocity as a function of frequency on 24 July 2003, for (a) case 1 at 0114:38 UT and (b) case 2 at 0135:25 UT. The obtained values of v_S display their corresponding error bars. Superimposed in both plots is the parallel velocity of resonant energetic electrons, $v_{||}$. In both cases the source is moving toward the spacecraft.

direction transverse to the magnetic field, but which are extended by as much as a few thousand kilometers along the magnetic field line so that different frequencies are emitted at different points along the field line.

[43] The source regions are found to be moving toward the observer in cases 1 and 2, which also happens to be toward the equator. The direction of propagation of the emitted chorus waves thus coincides with the direction of motion of the source, therefore leading to a positive Doppler shift in the measurements. In both cases 1 and 2 we have a rising chorus wave, i.e., a wave with frequency increasing in time. *Nunn et al.* [1997] established that the chorus emission is likely produced by a collective interaction of the wave with electrons distributed in both parallel velocity and pitch angle. Therefore the fact that a rising emission is observed cannot be uniquely related to the location of the source region with respect to the equator, without detailed information about the energetic particle distribution function.

[44] **Acknowledgments.** This research was supported by the National Aeronautics and Space Administration, under parent grant NAG5-9974 at the University of Iowa and with subcontract 4000061641 to Stanford University. We greatly appreciate the help of C. Abramo of DSN, and M. Hapgood of RAL in scheduling the real-time wideband data acquisition from the WBD receiver and also the help of J. H. Dowell, I. W. Christopher, J. M. Seeberger, and R. L. Brechwald of the University of Iowa in reducing the data to usable form. We thank P. M. E. Décréau, who has provided the Whisper data.

[45] Lou-Chuang Lee thanks Michel Parrot and another reviewer for their assistance in evaluating this paper.

References

Acton, F. S. (1990), *Numerical Methods That Work*, corrected ed., Math. Assoc. of Am., Washington, D. C.

Burtis, W. J., and R. A. Helliwell (1969), Banded chorus: A new type of VLF radiation observed in the magnetosphere by OGO-1 and OGO-3, *J. Geophys. Res.*, *74*(7), 3002–3010.

Burtis, W. J., and R. A. Helliwell (1976), Magnetospheric chorus: Occurrence patterns and normalized frequency, *Planet. Space Sci.*, *24*, 1007–1024.

Burton, R. K., and R. E. Holzer (1974), The origin and propagation of chorus in the outer magnetosphere, *J. Geophys. Res.*, *79*(7), 1014–1023.

Canu, P., et al. (2001), Identification of natural plasma emissions observed close to the plasmapause by the Cluster-Whisper relaxation sounder, *Ann. Geophys., Ser. B*, *19*(10–12), 1697–1709.

Décréau, P. M. E. (2001), Early results from the Whisper instrument on Cluster: An overview, *Ann. Geophys.*, *19*(10–12), 1241–1258.

Décréau, P. M. E., et al. (1997), Whisper, A resonance sounder and wave analyzer: Performances and perspectives for the Cluster mission, *Space Sci. Rev.*, *79*(1–2), 157–193.

Dunckel, N., and R. A. Helliwell (1969), Whistler-mode emissions on the OGO-1 satellite, *J. Geophys. Res.*, *74*(26), 6371–6385.

Etcheto, J., G. Belmont, P. Canu, and J. G. Trotignon (1983), Active sounder experiments on GEOS and ISEE, in *Active Experiments in Space*, *Proceedings of an International Symposium, Alpbach, Austria*, *Eur. Space Agency Spec. Publ., ESA-195*, 39–46.

Gendrin, R. (1974), Phase-bunching and other non-linear processes occurring in gyroresonant wave-particle interactions (in magnetosphere), *Astrophys. Space Sci.*, *28*, 245–266.

Gurnett, D. A., and B. J. O'Brien (1964), High-latitude geophysical studies with satellite Injun 3: 5. Very-low-frequency electromagnetic radiation, *J. Geophys. Res.*, *69*(1), 65–89.

Gurnett, D. A., R. L. Huff, and D. L. Kirchner (1997), The wide-band plasma wave investigation, *Space Sci.*, *79*, 195–208.

Gurnett, D. A., R. L. Huff, J. S. Pickett, A. M. Persoon, C. A. Kletzing, R. L. Mutel, I. W. Christopher, U. S. Inan, W. L. Martin, and J. L. Bougeret (2001), First results from the Cluster wide-band plasma wave investigation, *Ann. Geophys.*, *19*, 1259–1272.

Helliwell, R. A. (1965), *Whistlers and Related Ionospheric Phenomena*, Stanford Univ. Press, Stanford, Calif.

Helliwell, R. A. (1967), A theory of discrete VLF emissions from the magnetosphere, *J. Geophys. Res.*, *72*(19), 4773–4790.

Inan, U. S., and T. F. Bell (1977), The plasmapause as a VLF wave guide, *J. Geophys. Res.*, *82*(19), 2819–2827.

Inan, U. S., M. Platino, T. F. Bell, D. A. Gurnett, and J. S. Pickett (2004), Cluster measurements of rapidly moving sources of ELF/VLF chorus, *J. Geophys. Res.*, *109*(A5), A05214, doi:10.1029/2003JA010289.

Kennel, C. F., and H. E. Petschek (1966), Limit on stably trapped particle fluxes, *J. Geophys. Res.*, *71*(1), 1–28.

Lauben, D. S., U. S. Inan, T. F. Bell, D. Kirchner, G. B. Hospodarsky, and J. S. Pickett (1998), VLF chorus emissions observed by POLAR during the January 10, 1997, magnetic cloud, *Geophys. Res. Lett.*, *25*, 2995–2998.

Lauben, D. S., U. S. Inan, and T. F. Bell (2002), Source characteristics of ELF/VLF chorus, *J. Geophys. Res.*, *107*(A12), 1429, doi:10.1029/2000JA003019.

LeDocq, M. J., D. A. Gurnett, and G. B. Hospodarsky (1998), Chorus source locations from VLF Poynting flux measurements with the Polar spacecraft, *Geophys. Res. Lett.*, *25*, 4063–4066.

Levenberg, K. (1944), A method for the solution of certain problems in least squares, *Q. Appl. Math.*, *2*, 164–168.

Marquardt, D. (1963), An algorithm for least-squares estimation of nonlinear parameters, *J. Soc. Ind. Appl. Math.*, *11*, 431–441.

Moré, J. J., and M. Y. Cosnard (1979), Numerical solution of nonlinear equations, *Trans. Math. Software*, *5*(1), 64–85.

Nagano, I., S. Yagitani, H. Kojima, and H. Matsumoto (1996), Analysis of wave normal and Poynting vectors of the chorus emissions observed by Geotail, *J. Geomagn. Geoelectr.*, *48*(3), 299–307.

Nunn, D. (1974), A self-consistent theory of triggered VLF emissions, *Planet. Space Sci.*, *22*(3), 349–378.

Nunn, D., Y. Omura, H. Matsumoto, I. Nagano, and S. Yagitani (1997), The numerical simulation of VLF chorus and discrete emissions observed on the Geotail satellite using a Vlasov code, *J. Geophys. Res.*, *102*(A12), 27,083–27,098.

Omura, Y., D. Nunn, H. Matsumoto, and M. J. Rycroft (1991), A review of observational, theoretical and numerical studies of VLF triggered emissions, *J. Atmos. Terr. Phys.*, *53*(5), 351–358.

Parrot, M., O. Santolík, N. Cornilleau-Wehrlin, M. Maksimovic, and C. Harvey (2003), Magnetospherically reflected chorus waves revealed by ray tracing with CLUSTER data, *Ann. Geophys.*, *21*(5), 1111–1120.

Platino, M., U. S. Inan, T. F. Bell, D. A. Gurnett, J. S. Pickett, P. Canu, and P. M. E. Décréau (2005), Whistlers observed by the Cluster spacecraft outside the plasmasphere, *J. Geophys. Res.*, *110*(A3), A03212, doi:10.1029/2004JA010730.

Skoug, R. M., S. Datta, M. P. McCarthy, and G. K. Parks (1996), A cyclotron resonance model of VLF chorus emissions detected during electron microburst precipitation, *J. Geophys. Res.*, *101*(A10), 21,481–21,491.

Santolík, O., and D. A. Gurnett (2003), Transverse dimensions of chorus in the source region, *Geophys. Res. Lett.*, *30*(2), 1031, doi:10.1029/2002GL016178.

Santolík, O., D. A. Gurnett, J. S. Pickett, M. Parrot, and N. Cornilleau-Wehrlin (2003), Spatio-temporal structure of storm-time chorus, *J. Geophys. Res.*, *108*(A7), 1278, doi:10.1029/2002JA009791.

Santolík, O., D. A. Gurnett, J. S. Pickett, M. Parrot, and N. Cornilleau-Wehrlin (2004), A microscopic and nanoscopic view of storm-time chorus on 31 March 2001, *Geophys. Res. Lett.*, *31*(2), L02801, doi:10.1029/2003GL018757.

Sazhin, S. S., and M. Hayakawa (1992), Magnetospheric chorus emissions: A review, *Planet. Space Sci.*, *40*(5), 681–697.

Smith, A. J., and D. Nunn (1998), Numerical simulation of VLF risers, fallers, and hooks observed in Antarctica, *J. Geophys. Res.*, *103*(A4), 6771–6784.

Stix, T. H. (1962), *The Theory of Plasma Waves*, McGraw-Hill, New York.

Trakhtengerts, V. Y. (1999), A generation mechanism for chorus emission, *Ann. Geophys.*, *17*(1), 95–100.

Trotignon, J. G., J. Etcheto, and J. P. Thouvenin (1986), Automatic determination of the electron density measured by the relaxation sounder onboard ISEE 1, *J. Geophys. Res.*, *91*(A4), 4302–4320.

Trotignon, J. G., et al. (2001), How to determine the thermal electron density and the magnetic field strength from the Cluster/Whisper observations around the Earth, *Ann. Geophys.*, *19*, 1711–1720.

Trotignon, J. G., J. L. Rauch, P. M. E. Décréau, P. Canu, and J. Lemaire (2003), Active and passive plasma wave investigation in the Earth's environment: The CLUSTER/WHISPER experiment, *Adv. Space Res.*, *31*(5), 1449–1454.

T. F. Bell, U. S. Inan, and M. Platino, STAR Laboratory, Stanford University, 350 Serra Mall, Packard EE. Offfice 308, Stanford, CA 94305-9505, USA. (platinom@stanford.edu)

P. Canu, Centre d'Etudes des Environnements Terrestres et Planétaires, CNRS, Université Versailles Saint-Quentin-en-Yvelines, 10 avenue de l'Europe, F-78140 Vélizy Villacoublay, France.

J. S. Pickett, Department of Physics and Astronomy, 610 Van Allen Hall, Iowa City, IA 52242-0000, USA.